

New variable stars discovered in the fields of three Galactic open clusters using the VVV Survey

T. Palma^{a,b,c,*}, D. Minniti^{b,a}, I. Dékány^{a,d}, J.J. Clariá^{c,e}, J. Alonso-García^{f,a}, L.V. Gramajo^c, S. Ramírez Alegría^{a,g}, C. Bonatto^h

^a*Millennium Institute of Astrophysics, Chile*

^b*Departamento de Ciencias Físicas, Universidad Andrés Bello, Fernández Concha 700, 759-1598 Las Condes, Santiago, Chile*

^c*Observatorio Astronómico de Córdoba, Universidad Nacional de Córdoba, Laprida 854, X5000BGR, Córdoba, Argentina*

^d*Instituto de Astrofísica, Pontificia Universidad Católica de Chile, Av. Vicuña Mackenna 4860, 782-0436 Macul, Santiago, Chile*

^e*Consejo Nacional de Investigaciones Científicas y Técnicas (CONICET), Godoy Cruz 2290, CABA, C1425FQB, Argentina*

^f*Unidad de Astronomía, Facultad Cs. Básicas, Universidad de Antofagasta, Avda. U. de Antofagasta 02800, Antofagasta, Chile*

^g*Instituto de Física y Astronomía, Facultad de Ciencias, Universidad de Valparaíso, Av. Gran Bretaña 1111, Playa Ancha, Casilla 5030, Valparaíso, Chile*

^h*Universidade Federal do Rio Grande do Sul, Departamento de Astronomia, CP 15051, RS, 91501-970, Porto Alegre, Brazil*

Abstract

This project is a massive near-infrared (NIR) search for variable stars in highly reddened and obscured open cluster (OC) fields projected on regions of the Galactic bulge and disk. The search is performed using photometric NIR data in the J -, H - and K_s - bands obtained from the Vista Variables in the Vía Láctea (VVV) Survey. We performed in each cluster field a variability search using Stetson's variability statistics to select the variable candidates. Later, those candidates were subjected to a frequency analysis using the Generalized Lomb-Scargle and the Phase Dispersion Minimization algorithms. The number of independent observations range between 63 and 73. The newly discovered variables in this study,

*Corresponding author

Email addresses: `astrofisica.tp@unab.cl` (T. Palma), `dante@astrofisica.cl` (D. Minniti), `idekany@astro.puc.cl` (I. Dékány), `claria@oac.unc.edu.ar` (J.J. Clariá), `javier.alonso@uantof.cl` (J. Alonso-García), `luciana@oac.unc.edu.ar` (L.V. Gramajo), `sebastian.ramirez@uv.cl` (S. Ramírez Alegría), `charles.bonatto@ufrgs.br` (C. Bonatto)

157 in total in three different known OCs, are classified based on their light curve shapes, periods, amplitudes and their location in the corresponding color-magnitude ($J - K_s$, K_s) and color-color ($H - K_s$, $J - H$) diagrams. We found 5 possible Cepheid stars which, based on the period-luminosity relation, are very likely type II Cepheids located behind the bulge. Among the newly discovered variables, there are eclipsing binaries, δ Scuti, as well as background RR Lyrae stars. Using the new version of the Wilson & Devinney code as well as the “Physics Of Eclipsing Binaries” (PHOEBE) code, we analyzed some of the best eclipsing binaries we discovered. Our results show that these studied systems turn out to be ranging from detached to double-contact binaries, with low eccentricities and high inclinations of approximately 80° . Their surface temperatures range between 3500K and 8000K.

Keywords: Galaxy: stellar content – open clusters and associations: individual: Antalova 1, ASCC 90, ESO 393-15 – stars: variables: general

1. Introduction

Star clusters are important building blocks of galaxies so knowledge of their individual and statistical properties is of great astrophysical importance. These populations, composed of stars sharing the same age and initial chemical composition, have allowed us to test theories of stellar evolution and have also helped to reveal the structure of their host galaxies. In particular, Galactic open clusters (OCs) have long been considered excellent targets not only to probe the Galactic disk population (Friel, 1995; Bica et al., 2006) but also to trace its chemical evolution (see, e.g., Chen et al., 2003, and references therein). Estimates indicate that the Milky Way currently hosts a total of about 2.5×10^4 or more OCs (Portegies Zwart et al., 2010). However, in the catalogue by Kharchenko et al. (2013, hereafter K13), only 2808 Galactic OCs have reasonable estimates of basic cluster parameters such as distance and age, as well as an estimation of the interstellar extinction. This number clearly represents a lower limit to the possible amount of clusters belonging to the Milky Way, if we take into account the recently found clusters and cluster candidates (see, e.g., Bica et al., 2003; Dutra et al., 2003; Borissova et al., 2011, 2014; Ramírez Alegría et al., 2014, 2016; Chené et al., 2013; Barbá et al., 2015) and the “still unseen” OCs, which are deeply embedded in obscured regions or are just too faint to be detected. Distances, masses, and ages for OCs are generally determined from color-magnitude diagrams (CMDs). However, observations of OCs projected on the Galactic bulge region are strongly

affected by the effects of both interstellar reddening and high field stellar density (Valenti et al., 2007; Alonso-García et al., 2012). In these objects, the cluster main sequences appear not to be clearly visible, which reduces the accuracy of the relevant physical parameters derived from their CMDs. In these cases, it is very helpful to identify cluster member variable stars since these stars can provide a more precise measurement of the clusters' parameters (particularly their distances).

The current project, based on near-infrared (NIR) photometric data, is a search for stellar variability in the fields of Galactic OCs which lie in the highly reddened and obscured regions of the Galactic bulge and disk. As part of a massive search for variable stars in OCs, we characterize for the first time new variable stars detected in three Galactic OC regions located toward the inner Galaxy. For this purpose, we make use of the VISTA Variables in the Vía Láctea (VVV) Survey, which is an ESO Public NIR time-domain survey of the inner Milky Way (Minichiello et al., 2010). VVV aims to map the Galactic bulge as well as an adjacent section of the mid-plane, covering stellar populations all the way to the Galactic center, including regions of intense star formation. This survey has been performing time-domain observations in the K_s -band for over 5 years (Saito et al., 2012) and provides an atlas of 562 square degrees of the sky in 5 wavebands ($ZYJHK_s$), encompassing about a billion objects.

The VVV Survey is discovering hundreds of new clusters, many of them being very distant and deeply embedded objects toward the inner Galaxy (see, e.g., Borissova et al., 2011, 2014; Chené et al., 2013; Ramírez Alegría et al., 2014, 2016). The relevant physical parameters (reddenings, distances, masses, luminosities, sizes and metallicities) for these new clusters are still poorly known or unknown. Our project aims at focusing on all OCs in the VVV survey area. In this first approach, we analyze a few known OCs with previously identified variables. We selected, on the one hand, two moderately young and extended OCs with a relatively high amount of catalogued variables in their fields (Zejda et al., 2012) and a considerable amount of new possible variable member candidates. On the other hand, we also selected an intermediate-age more compact OC with only a few known variable stars and some newly discovered variable candidates detected in our study. Because the clusters are projected onto high density stellar regions of the Galactic bulge, we are at present mainly focused on searching probable NIR counterparts of the already catalogued variable stars as well as searching new variables only discovered using the VVV data. The subsequent goals will be related

to the clusters' analysis, i.e., to comparing the advantages and disadvantages of analyzing extended and compact OCs and selecting close and faint OCs to warrant their non saturation and usefulness for a future analysis of their proper motions. In addition, with the help of our new data, we aim at improving some of these clusters' parameters that appeared to be uncertain.

In this work we present the first results obtained for three OCs projected on the inner parts of the Galactic bulge, namely Antalova 1, ASCC 90 and ESO 393-15. We describe them in the next section together with the data collected from the VVV Survey. Section 3 details the variable stars found in the fields of these three OCs and their classification based on the obtained light curves. Data analysis and discussion as well as some future work is described in Section 4.

2. Data acquisition and selected targets

The observations were made as part of the VVV Survey. The VIRCAM camera on the 4.1 m VISTA telescope is an array of 16 NIR detectors which produce a combined image of $11.6' \times 11.6'$ with a pixel size of $0.34''$ (Dalton et al., 2006). The photometry and data reduction have been described in detail elsewhere (Saito et al., 2012; Dékány et al., 2013; Alonso-García et al., 2015). We briefly mention here that the individual VVV images were reduced, astrometrized and stacked by the Cambridge Astronomy Survey Unit (CASU) using the VISTA Data Flow System (VDFS) pipeline (Emerson et al., 2004; Irwin et al., 2004; Hambly et al., 2004), and the photometry has been calibrated onto the VISTA filter system. The aperture photometry has been made by CASU on the individual processed images, and generated light curves were then analyzed for variability (see Dékány et al., 2013; Alonso-García et al., 2015). PSF photometry for each OC in the different available images was extracted and later cross-matched to create the CMDs. A brief description of the selected targets as well as a summary of the previous results for the fields under investigation is given below.

2.1. *Antalova 1*

Antalova 1 (IAU designation C1725-315) is catalogued as a moderately young and metal-poor OC located in Scorpius at $\alpha_{2000} = 17^{\text{h}} 28^{\text{m}} 57^{\text{s}}$, $\delta_{2000} = -31^{\circ} 34' 48''$; $l = 355.86^{\circ}$, $b = +1.64^{\circ}$ (K13). It is projected on the inner bulge in the area named b345 in Saito et al. (2012). Antalova 1 has been classified as IV2pn in the

Trumpler system (Archinal and Hynes, 2003), i.e., as an OC with the fourth highest concentration degree, a medium range of brightness of its stars and a scanty population. Kharchenko et al. (2005b, hereafter K05) published a catalogue of astrophysical data for 520 Galactic OCs - among them Antalova 1 - which could be identified in their All-Sky Compiled Catalogue of 2.5 million stars (ASCC-2.5). By applying homogeneous procedures and algorithms, K05 determined angular sizes and fundamental astrophysical parameters for their cluster sample. For Antalova 1, they estimated an angular radius of $35'$, and obtained the following results: $E(B-V) = 0.25$, $d = 850$ pc and 316 Myr. It should be noted, however, that owing to the relatively bright limiting magnitude ($V \sim 12.5$) of the ASCC-2.5, K05's sample does not include faint and generally remote or highly obscured OCs. More recently, using a combination of uniform kinematic and NIR photometric data gathered in the all-sky catalogue PPMXL (Roeser et al., 2010) and the 2MASS catalogue (Skrutskie et al., 2006), K13 reported exact positions, apparent radii, proper motions, reddenings, distances and ages for more than 2800 mostly confirmed OCs. For Antalova 1, they provided the parameters listed in Table 1. Conrad et al. (2014) identified Antalova 1 in the Radial Velocity Experiment (RAVE; Steinmetz et al., 2006) and determined its mean cluster metallicity as $[M/H] = -0.66 \pm 0.19$ (Table 1) from a cleaned working sample. A total of 43 variable stars have been catalogued by Zejda et al. (2012, hereafter Z12) in the cluster field.

2.2. ASCC 90

ASCC 90, also known as KPR 90 (Kharchenko et al., 2005a), has so far received little attention. This cluster is also situated in Scorpius at equatorial coordinates $\alpha_{2000} = 17^{\text{h}} 39^{\text{m}} 07^{\text{s}}$, $\delta_{2000} = -34^{\circ} 48' 54''$ and Galactic coordinates $l = 354.29^{\circ}$ and $b = -1.91^{\circ}$. It is projected into the region named b301 in Saito et al. (2012). K05 obtained for ASCC 90 the following results: $E(B - V) = 0.30$, $d = 500$ pc and age = 646 Myr, which are nearly identical to those recently provided by K13. Z12 reported a total of 62 variable stars in the field of ASCC 90. No metallicity has been determined for this cluster up to now.

2.3. ESO 393-15

ESO 393-15 (C1740-342) is an intermediate-age (1.4 Gyr) OC located in a rich stellar field in Scorpius at $\alpha_{2000} = 17^{\text{h}} 43^{\text{m}} 35^{\text{s}}$, $\delta_{2000} = -34^{\circ} 13' 38''$ and $l = 355.26^{\circ}$ and $b = -2.40^{\circ}$. This is a Trumpler (1930) class III3 OC (Archinal and

Table 1: Open cluster coordinates

ID	α_{2000} [hms]	δ_{2000} [dms]	l [d]	b [d]	tile
Antalova 1	17:28:57.0	-31:34:48	355.833	+01.625	b345
ASCC 90	17:39:07.2	-34:48:54	354.290	-01.910	b301-b302
ESO 393-15	17:43:35.3	-34:13:38	355.261	-02.396	b302

Table 2: Open cluster known parameters taken from Kharchenko et al. (2013).

ID	Radius [arcmin]	Dist [pc]	$E(J - K_s)$ [mag]	$\log t$ [yr]	PM_α [mas/yr]	PM_δ [mas/yr]	RV [km/s]	[Fe/H] [dex]
Antalova 1	14.1	930	0.205	8.485	-0.60	2.73	-2.8	-0.655
ASCC 90	18.3	526	0.144	8.81	-3.00	-3.65	–	–
ESO 393-15	5.4	2471	0.800	9.15	-9.15	0.23	–	–

Hynes, 2003), i.e. a moderately populated cluster with no noticeable concentration and a medium range in the star brightness. ESO 393-15 lies in the area b302 of Saito et al. (2012). According to K13, this cluster is a small sized object with an angular diameter of 5.4', located at 2471 pc from the Sun and affected by $E(B - V) = 1.67$. Z12 reported five variable stars in the cluster's field. No metallicity estimate has so far been obtained for this cluster.

Table 1 lists the coordinates of the clusters and their locations in the VVV area, while Table 2 summarizes the fundamental parameters of the selected targets reported by K13, including their apparent radii, distances, reddenings, ages, proper motions, radial velocities and metallicities, when available.

The $(J - K_s, K_s)$ CMDs as well as $(H - K_s, J - H)$ color-color diagrams were built for each OC. As can be seen in Figures 1 - 3, the clusters are projected onto high stellar density regions where the Galactic disk and bulge populations greatly contaminate the clusters' CMDs (grey dots). A decontamination procedure was required in order to detect and separate clusters from their background stars. With this in mind, we applied a statistical method consisting in defining a ring region surrounding each cluster located 5' away from its field and considered it as a comparison field and counted the stars lying within different intervals of magnitude-color $[\delta K_s, \delta(J - K_s)]$ in the CMD of each selected region. Finally, the number of stars counted for each interval $[\delta K_s, \delta(J - K_s)]$ in the CMD of the

comparison fields was subtracted from the number of stars of the corresponding cluster regions. This procedure, applied successfully to other more compact clusters, failed to yield the expected results. It could be argued that at least in two of the three studied objects, the failure of the cleaning method may be due to the fact that these two OCs are not concentrated and are also very extended, so the separation between cluster and field stars is more confusing. In Figures 1 - 3 we marked with black dots the stars that remain after the decontamination procedure. As can be seen in the upper-right panel, a strange X-shape appears as resembling two different stellar populations. We believe that the bulge main sequence seen in the color-magnitude diagrams (star concentration at $K_s > 16$ approximately) is the responsible for such feature. By subtracting this stellar population, the color-magnitude and color-color diagrams of the two lower panels in Figures 1 - 3 are obtained. Dark grey points most probably represent the red giant branch of the background bulge older stellar population. Isochrone fittings from Bressan et al. (2012) were superimposed on the CMDs (red lines) based on cluster ages, distances, reddenings, and metallicities (when published) from K13. We compare with the reddening maps of Gonzalez et al. (2011) and Gonzalez et al. (2012) obtained with the VVV data, but since those maps were calculated for the bulge distances, the values represent an upper limit for the possible clusters reddenings.

3. Variability analysis

For each cluster field, we extracted and analyzed VVV data for objects that best matched the positions of previously reported variable stars (Z12), and also performed a blind variability search. Objects with putative light variations were selected using Stetson's variability statistics (Stetson, 1996). The preselected candidates ($\sim 10\%$ of the objects) were then subjected to a frequency analysis. Signal detection was performed using the Generalized Lomb-Scargle (GLS; Zechmeister and Kürster, 2009) and the Phase Dispersion Minimization (PDM; Stellingwerf, 1978) algorithms. Phase-folded light curves with the resulting preliminary periods were then visually inspected to select the best solution and to reject spurious signals resulting from various systematics, e.g., rotating diffraction spikes of nearby saturated stars.

We refined the periods and optimized the light-curve fit by an iterative procedure including the steps of outlier rejection, aperture optimization, determination of the optimal order of the best-fitting Fourier sum, and refining the period by a

non-linear least squares method. The mean apparent K_s magnitudes of the stars and the total amplitudes of the light curves were computed from the final Fourier solutions. At the end of the process, we identified a total of 157 variable stars with the number of independent observations ranging between 63 and 73.

The classification of periodic variable stars in this study was based on the periods and amplitudes, on visual appearance of the light curves and on the objects' color indices. Classifying NIR light curves is not a straightforward procedure because K_s -band light-curves of pulsating variable stars have typically smaller amplitudes and are much more featureless than in the optical region, making it difficult to distinguish different types of objects on the basis of NIR data alone.

The catalogue of Z12 reports variable stars found in the fields of the three selected clusters. However, by cross-matching their coordinates with the VVV source catalog, we have not found any variable star with NIR counterpart in any of the three fields. We attribute that to the fact that most of the catalogued variables are bright stars, so they are saturated on the VVV K_s -band. Other variable stars might also have amplitudes too low to be detected in our procedure as possible variables.

In the field of Antalova 1, we detected 58 new variable stars from which 7 are newly possible RR Lyrae type stars, 3 were classified as possible Cepheids and 18 as probable eclipsing binary (EB) systems. The remaining ones are reliably classified as undefined types of variable stars (denoted as MISC or marked with asteriks) or stars whose periods could not be well determined. Their coordinates, periods, amplitudes, $\langle K_s \rangle$ weighted mean magnitudes from the Fourier fit, $J - K_s$ and $H - K_s$ colors computed from the first K_s -band epoch, and classifications are given in Table 3. In the field of ASCC 90, we have detected 81 new variable stars. Out of these, 10 are found to be possible RR Lyrae, 2 suspected Cepheids and 1 possible δ Scuti, while 43 are found to have similar characteristics to EB systems. Their basic properties are detailed in Table 4. In the field of ESO 393-15, we identified 18 new variable stars from which 2 are classified as RR Lyrae stars, 1 as possible δ Scuti star, 1 as ellipsoidal and 8 as binary systems. We show in Table 5 the corresponding parameters and classifications for all the variable stars found in this field.

Figure 4 shows a schematic view in the period-amplitude plane (Bailey diagram) of the whole sample of newly identified variables in the CMDs of the three

studied OCs. Symbols are the same as in Fig. 4. Figures 5-7 show the light curves obtained for all the well classified variables, i.e., variables with Alias periods are not included.

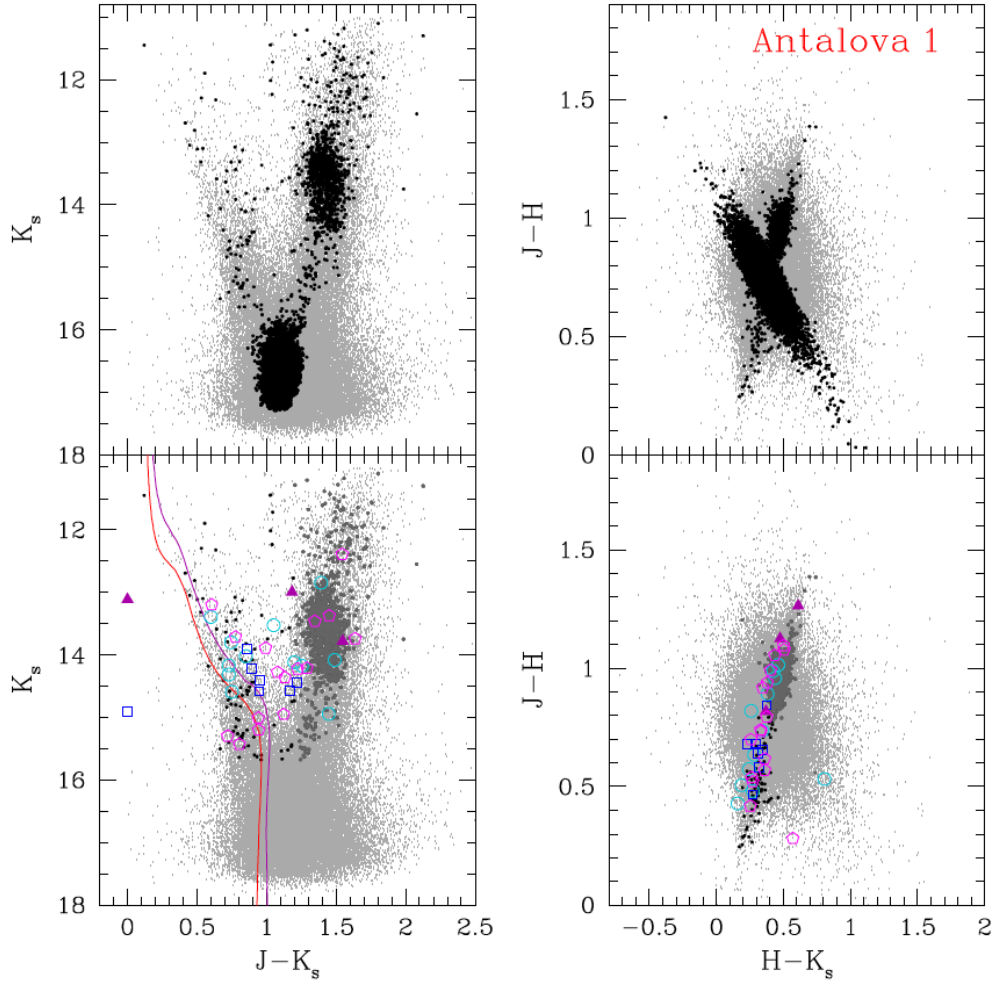


Figure 1: Color- magnitude and color-color diagrams of Antalova 1. Grey dots indicate all stars within the clusters' radii, while black dots represent stars that remain after the decontamination procedure. In the bottom diagrams, we subtracted also the clear bulge main-sequence background and fitted with a red line the Bressan et al. (2012) isochrone corresponding to the parameters estimated by K13. The corresponding solar metallicity isochrone is represented by the purple line. Dark grey points represent the bulge red giant branch. We also superimposed on the diagrams the variable stars found in the cluster field. Different symbols and colors represent different types of variables.

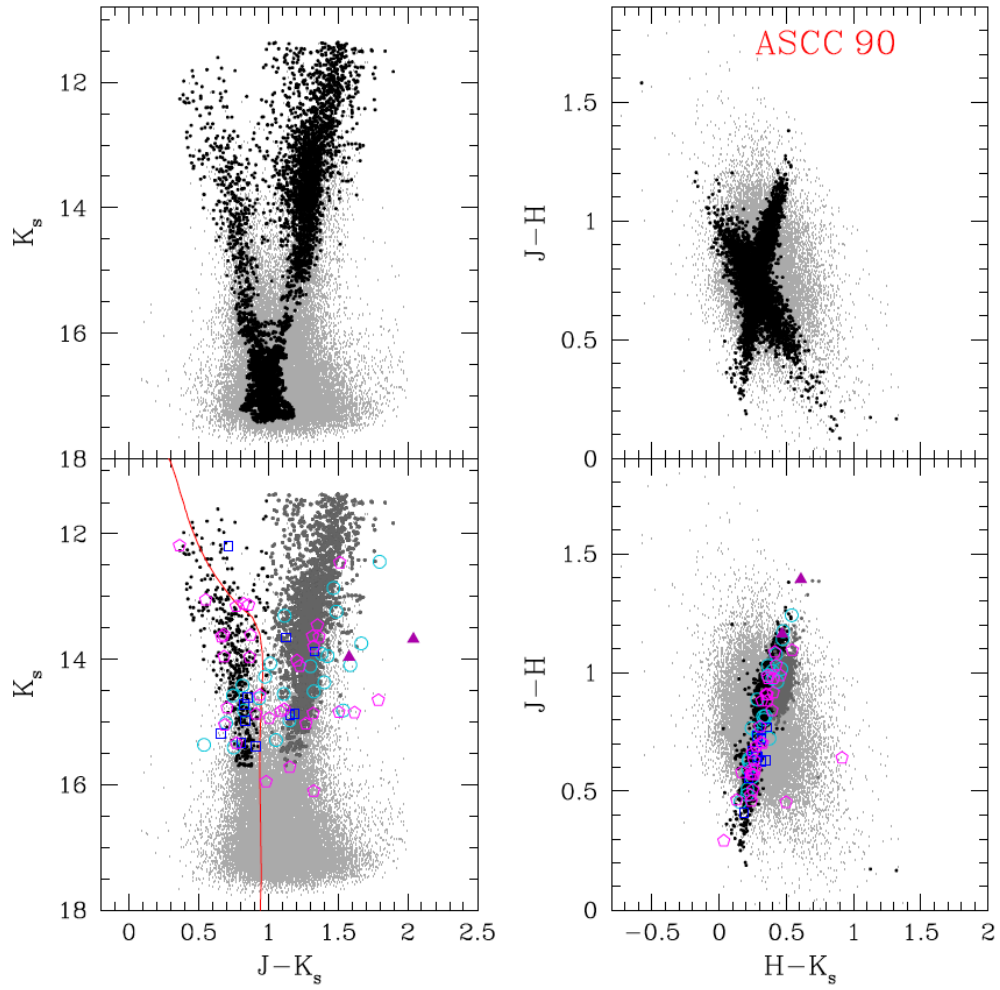


Figure 2: Same as Figure 1 but for ASCC 90.

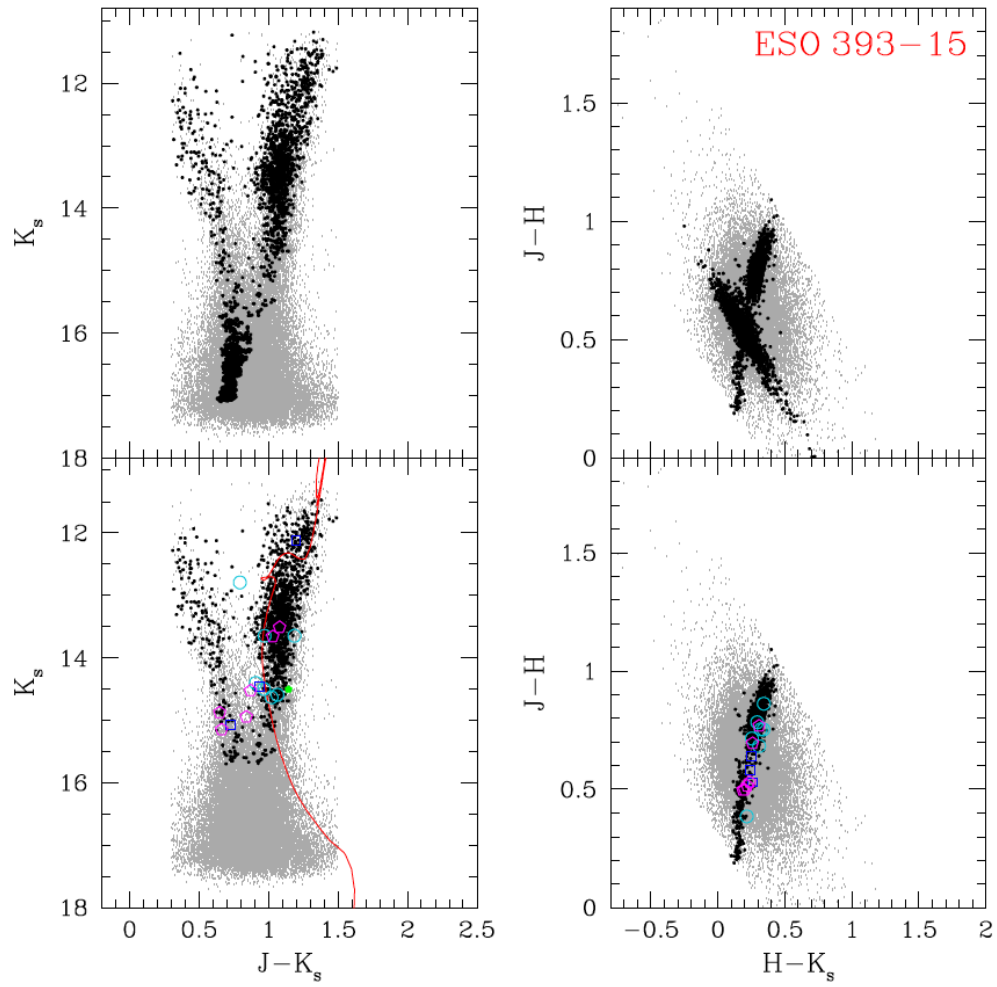


Figure 3: Same as Figure 1 but for ESO 393-15.

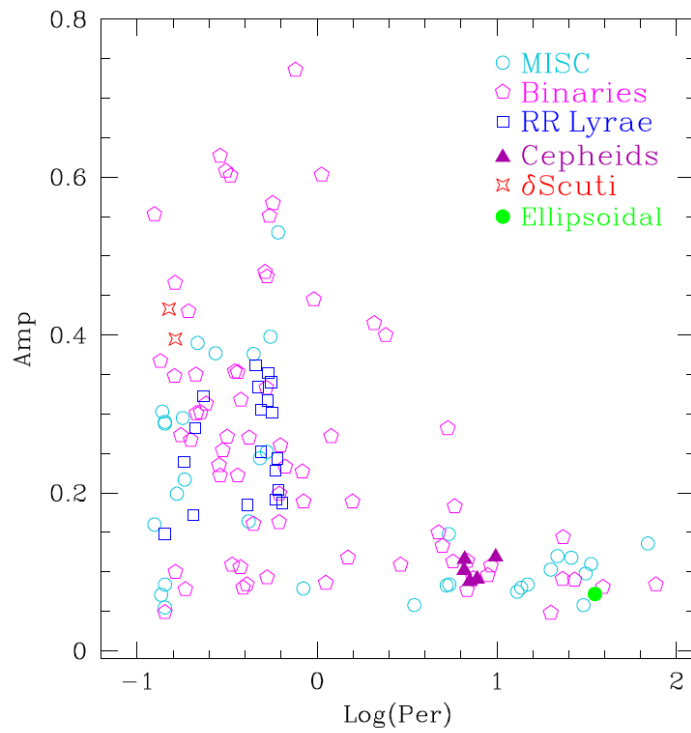


Figure 4: Distribution of the new variables in the period-amplitude plane. Different symbols and colors represent the various types of variables.

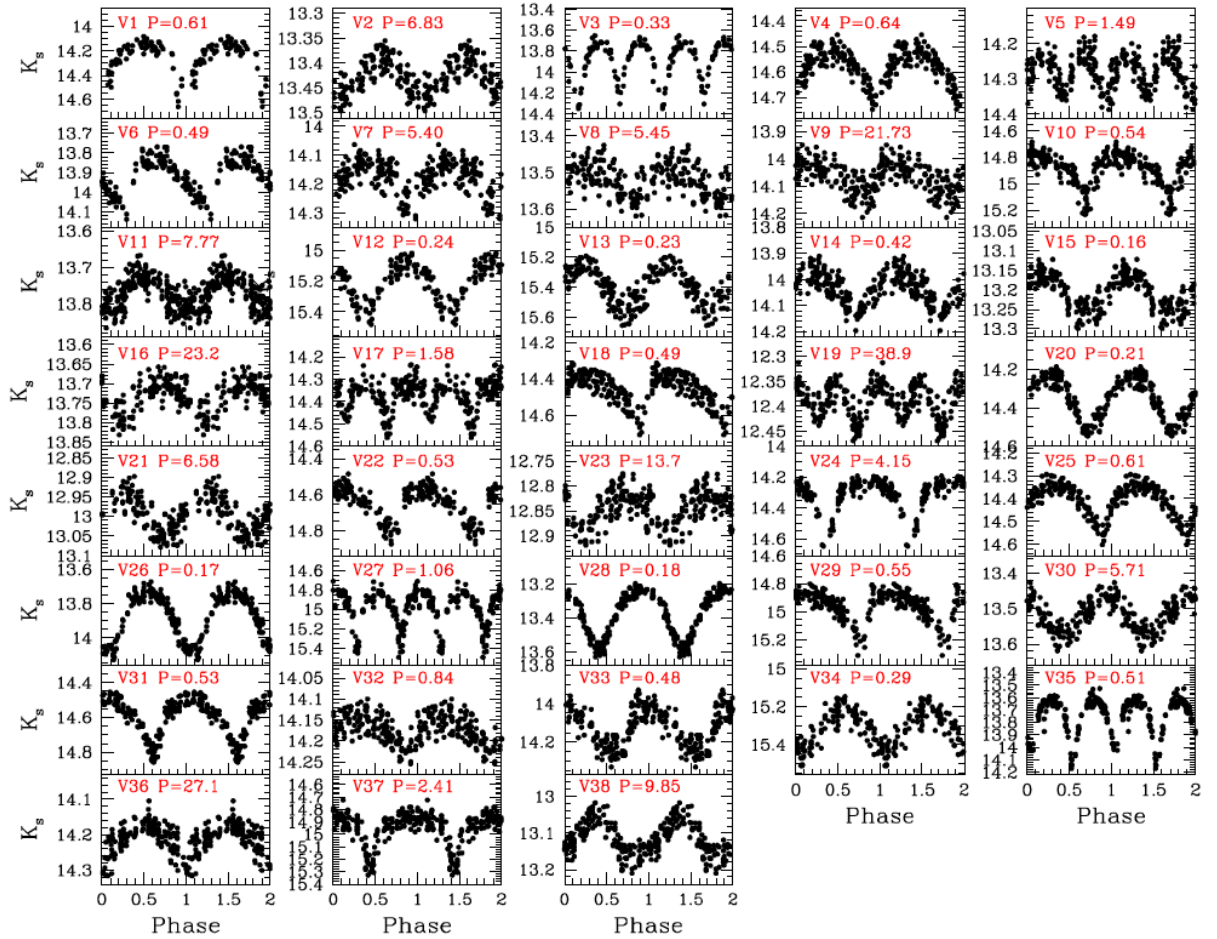


Figure 5: Light curves of the variable stars found in the field of Antalova 1

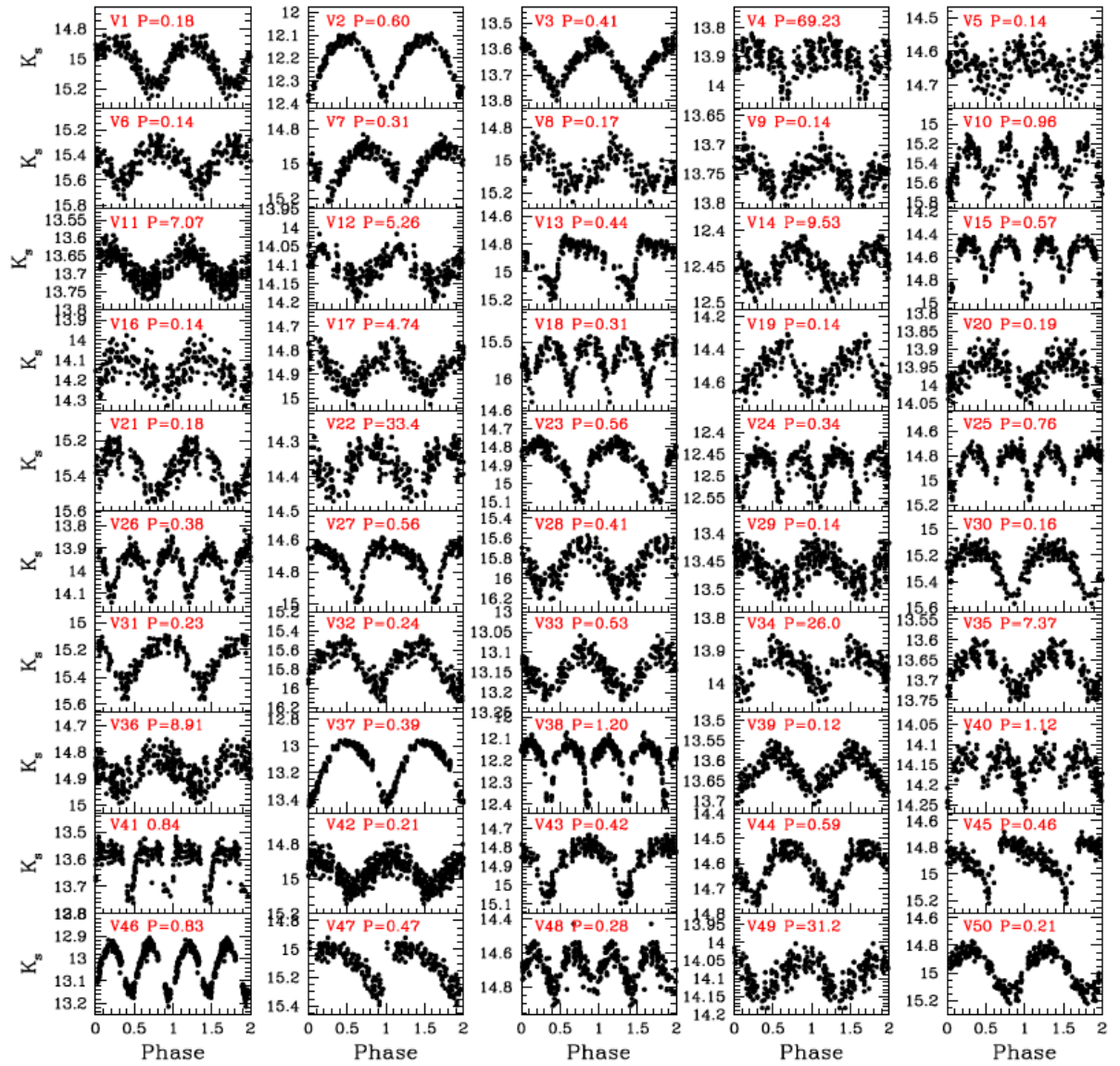


Figure 6: Light curves of the variable stars found in the field of ASCC 90

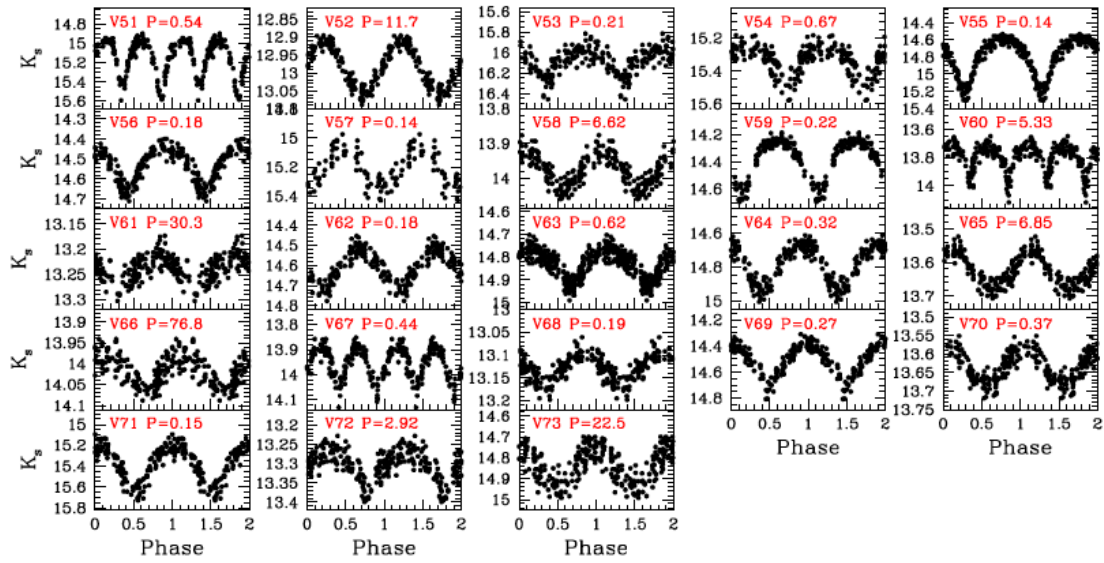


Figure 6: Continued.

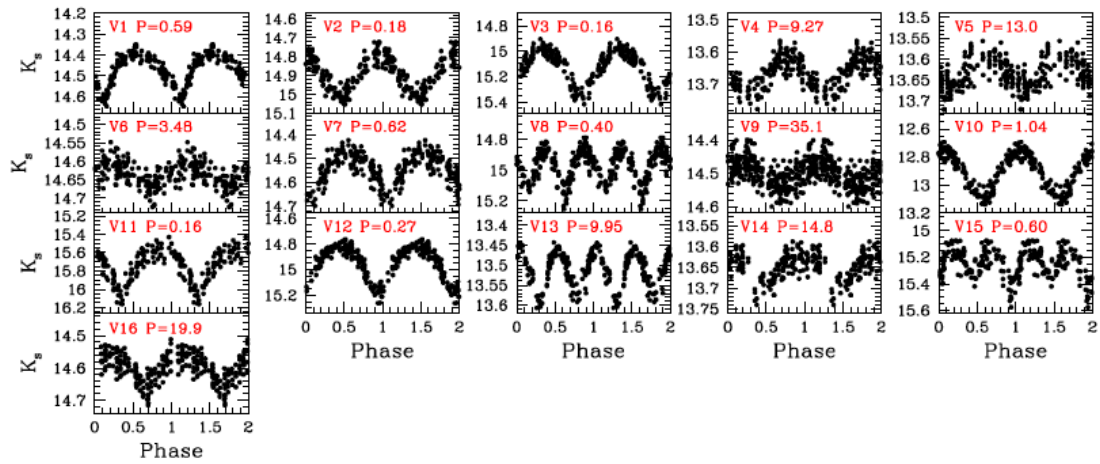


Figure 7: Light curves of the variable stars found in the field of ESO 393-15

Table 3: List of variable stars found in Antalova I

ID	α_{2000} [hms]	δ_{2000} [dms]	Dist ^a [arcmin]	Period [days]	Amp ^b [mag]	$\langle K_s \rangle$ [mag]	$J - K_s$ [mag]	$H - K_s$ [mag]	Class	Comments (other types/periods)
V1	17:28:26.70	-31:29:39.0	5.17	0.60804	0.530	14.24	0.82	0.24	MISC	...
V2	17:28:43.23	-31:30:50.9	10.97	6.82885	0.077	13.43	1.49	0.44	Bin	Ellipsoidal
V3	17:28:46.35	-31:25:00.9	9.79	0.33013	0.602	13.88	0.96	0.26	Bin	...
V4	17:28:47.57	-31:28:55.0	5.89	0.63813	0.187	14.58	1.22	0.38	RR*	Bin
V5	17:28:50.93	-31:28:55.2	5.88	1.48478	0.118	14.28	1.07	0.33	Bin	RR; P=0.74298 d
V6	17:28:51.09	-31:28:37.2	6.18	0.48991	0.305	13.92	0.90	0.32	RR	...
V7	17:28:53.84	-31:33:35.8	1.20	5.40317	0.148	14.18	0.81	0.27	MISC	...
V8	17:28:53.87	-31:31:45.9	3.04	5.44742	0.084	13.52	1.08	0.26	MISC	Spheroidal*
V9	17:28:54.68	-31:23:55.8	10.87	21.73366	0.120	14.06	1.48	0.46	MISC	...
V10	17:28:58.37	-31:22:58.6	11.82	0.53609	0.352	14.89	0.91	0.23	RR	Bin
V11	17:29:00.89	-31:21:39.0	13.15	7.77096	0.091	13.77	1.60	0.48	Cep*	MISC
V12	17:29:01.74	-31:26:39.5	8.14	0.24126	0.313	15.21	0.85	0.57	Bin	...
V13	17:29:06.70	-31:31:22.3	3.43	0.22554	0.302	15.39	0.93	0.36	Bin	...
V14	17:29:11.64	-31:33:26.8	1.38	0.41652	0.164	14.04	0.75	0.27	MISC	...
V15	17:29:12.51	-31:23:24.4	11.40	0.16319	0.100	13.21	0.67	0.25	Bin	...
V16	17:29:13.03	-31:30:21.8	4.44	23.20854	0.091	13.73	1.60	0.50	Bin	...
V17	17:29:14.26	-31:27:32.2	7.27	1.57594	0.189	14.37	0.98	0.36	Bin	...
V18	17:29:14.47	-31:35:31.0	0.77	0.48816	0.252	14.47	1.00	0.35	RR	...
V19	17:29:16.09	-31:27:11.2	7.62	38.92414	0.081	12.39	1.58	0.51	Bin	...
V20	17:29:16.24	-31:17:19.1	17.48	0.21118	0.282	14.35	0.74	0.27	RR	...
V21	17:29:16.38	-31:26:55.8	7.88	6.58358	0.102	12.99	1.19	0.37	Cep*	...
V22	17:29:16.87	-31:16:55.7	17.87	0.52663	0.252	14.65	0.92	0.28	MISC	...
V23	17:29:17.45	-31:32:09.3	2.67	13.66544	0.080	12.85	1.40	0.44	MISC	...
V24	17:29:18.23	-31:25:38.5	9.17	2.07537	0.415	14.33	1.17	0.38	Bin	...
V25	17:29:18.29	-31:35:42.0	0.97	0.60952	0.204	RR	14.41	0.97	0.29	Bin
V26	17:29:18.75	-31:21:26.7	13.36	0.17437	0.354	13.87	0.69	0.19	MISC	Bin; P=0.34874
V27	17:29:20.22	-31:35:36.5	0.90	1.06129	0.603	14.96	1.07	0.33	Bin	P=0.53066
V28	17:29:21.23	-31:21:43.8	13.08	0.18109	0.353	13.36	0.59	0.16	MISC	Bin; P=0.36216
V29	17:29:22.00	-31:31:07.1	3.71	0.55032	0.398	14.97	1.27	0.38	MISC	...
V30	17:29:22.17	-31:35:01.1	0.47	5.70666	0.113	13.52	1.32	0.38	Bin	...
V31	17:29:24.16	-31:28:27.7	6.35	0.53211	0.317	14.59	0.95	0.31	RR/Bin	...
V32	17:29:26.25	-31:34:25.8	0.61	0.83882	0.079	14.17	1.41	0.42	MISC	...
V33	17:29:29.30	-31:37:16.6	2.53	0.48178	0.244	14.12	1.08	0.34	MISC	...
V34	17:29:29.90	-31:30:52.7	3.96	0.28913	0.222	15.31	0.79	0.27	Bin	MISC
V35	17:29:31.07	-31:25:01.1	9.80	0.51328	0.480	13.82	0.80	0.26	Bin	...
V36	17:29:31.57	-31:36:04.7	1.40	27.07240	0.090	14.21	1.40	0.40	Bin	MISC
V37	17:29:34.09	-31:33:05.4	1.82	2.40947	0.400	14.95	1.26	0.35	Bin	...
V38	17:29:35.26	-31:34:58.1	0.66	9.85270	0.119	13.11	1.87	0.61	Cep*	...
V39	17:28:29.67	-31:29:05.4	5.73	...	0.236	13.93	1.86	0.61	MISC	...
V40	17:28:32.97	-31:30:24.2	4.41	...	0.305	14.43	1.80	0.63	MISC	...
V41	17:28:53.86	-31:28:31.8	6.27	...	0.227	14.90	1.40	0.43	MISC	...
V42	17:28:58.92	-31:21:40.4	13.13	...	0.162	12.74	0.69	0.34	MISC	...
V43	17:29:01.23	-31:34:01.9	0.77	...	0.306	14.19	1.23	0.44	MISC	...
V44	17:29:02.51	-31:33:52.3	0.93	...	0.298	12.99	1.61	0.57	MISC	...
V45	17:29:03.44	-31:20:31.7	14.27	...	0.110	12.99	1.46	0.50	MISC	...
V46	17:29:03.67	-31:33:37.5	1.18	...	0.387	14.72	1.25	0.50	MISC	...
V47	17:29:05.37	-31:30:22.0	4.44	...	0.303	14.34	1.73	0.59	MISC	...
V48	17:29:06.48	-31:31:57.1	2.85	...	0.278	14.28	1.08	0.31	MISC	...
V49	17:29:09.50	-31:28:01.6	6.78	...	0.346	14.67	1.43	0.59	MISC	...
V50	17:29:11.58	-31:34:18.9	0.54	...	0.561	13.77	2.06	0.71	MISC	...
V51	17:29:13.84	-31:21:55.6	12.88	...	0.257	13.76	1.36	0.39	MISC	...
V52	17:29:2.84	-31:34:28.6	0.57	...	0.132	14.44	1.27	0.45	MISC	...
V53	17:29:25.01	-31:31:54.8	2.92	...	0.230	14.45	1.29	0.41	MISC	...

Table 3: Continued.

ID	α_{2000} [hms]	δ_{2000} [dms]	Dist ^a [arcmin]	Period [days]	Amp ^b [mag]	$\langle K_s \rangle$ [mag]	$J - K_s$ [mag]	$H - K_s$ [mag]	Class	Comments (other types/periods)
V54	17:29:25.11	-31:34:52.0	0.47	...	0.443	15.01	1.65	...	MISC	...
V55	17:29:29.68	-31:21:45.2	13.06	...	0.205	14.48	MISC	...
V56	17:29:31.32	-31:22:33.1	12.26	...	0.219	13.95	0.85	0.41	MISC	...
V57	17:29:34.02	-31:38:55.2	4.17	...	0.130	14.14	1.08	0.36	MISC	...
V58	17:29:35.60	-31:31:19.2	3.54	...	0.430	14.24	0.96	0.27	MISC	...

^a Distance to the cluster center. ^b K_s total amplitude.

Table 4: List of variable stars found in ASCC 90

ID	α_{2000} [hms]	δ_{2000} [dms]	Dist ^a [arcmin]	Period [days]	Amp ^b [mag]	iK_s [mag]	$J - K_s$ [mag]	$H - K_s$ [mag]	Class	Comments (other types/periods)
V1	17:37:56.45	-34:49:51.1	17.71	0.17500	0.273	15.02	0.75	0.17	Bin	δ Sct
V2	17:37:57.42	-34:50:46.3	17.55	0.60235	0.244	12.21	0.59	0.18	RR/Bin	...
V3	17:38:00.24	-34:43:10.0	17.69	0.41059	0.185	13.65	1.02	0.28	RR/Bin	...
V4	17:38:04.41	-34:49:15.8	15.70	69.23252	0.136	13.91	1.39	0.43	MISC	...
V5	17:38:06.23	-34:44:11.2	15.96	0.13602	0.071	14.64	0.81	0.22	MISC	...
V6	17:38:09.52	-34:41:55.3	16.02	0.13791	0.303	15.45	1.17	0.28	MISC	...
V7	17:38:12.52	-34:50:02.1	13.72	0.31308	0.260	15.00	0.69	0.21	MISC	Bin; P=0.62616
V8	17:38:16.80	-34:41:22.3	14.68	0.16621	0.199	15.05	1.40	0.40	MISC	...
V9	17:38:16.81	-34:40:58.5	7.07	0.14247	0.055	13.75	1.65	0.48	MISC	...
V10	17:38:23.72	-34:48:19.2	10.89	0.47946	0.445	15.43	0.72	0.21	MISC	Bin; P=0.95893
V11	17:38:27.14	-34:35:38.8	16.62	7.06969	0.088	13.68	2.00	0.61	Cep*	...
V12	17:38:28.74	-34:40:22.0	12.86	5.26004	0.083	14.10	1.35	0.36	MISC	...
V13	17:38:30.78	-34:44:38.8	10.05	0.44373	0.376	14.90	1.00	0.24	MISC	...
V14	17:38:32.66	-34:35:32.7	15.91	9.52668	0.048	12.45	1.78	0.54	MISC	Bin; P=19.04586
V15	17:38:34.82	-34:33:26.9	17.44	0.56796	0.567	14.63	1.02	0.32	Bin	...
V16	17:38:35.83	-34:38:45.9	12.81	0.14247	0.148	14.15	1.04	0.32	RR	δ Sct*
V17	17:38:41.52	-34:45:55.7	7.07	4.73548	0.150	14.88	1.35	0.36	Bin	...
V18	17:38:41.67	-34:33:26.0	16.73	0.31084	0.608	15.72	1.20	0.32	Bin	...
V19	17:38:42.87	-34:49:42.6	16.73	0.14247	0.290	14.52	1.14	0.33	MISC	...
V20	17:38:43.33	-34:36:14.5	14.00	0.19380	0.080	13.96	1.03	0.29	MISC	Bin; P=0.38759
V21	17:38:43.55	-34:46:41.7	6.31	0.17915	0.295	15.36	0.85	0.22	MISC	...
V22	17:38:46.21	-34:32:11.7	17.51	33.44160	0.110	14.37	1.39	0.36	MISC	...
V23	17:38:49.38	-34:44:55.2	5.97	0.56232	0.302	14.88	1.13	0.36	RR*	...
V24	17:38:49.64	-34:44:42.2	6.07	0.33683	0.109	12.45	1.46	0.42	Bin	P=0.16841
V25	17:38:51.49	-34:43:57.4	6.31	0.75759	0.648	14.87	0.30	1.08	Bin	...
V26	17:38:52.06	-34:46:41.9	11.29	0.37722	0.220	14.00	0.95	0.50	Bin	P=0.18861
V27	17:38:52.21	-34:34:44.1	14.65	0.55657	0.340	14.73	0.95	0.28	RR*	Bin
V28	17:38:54.31	-34:49:44.8	3.33	0.40672	0.390	15.85	0.68	0.17	Bin	...
V29	17:38:57.99	-34:49:25.8	2.36	0.14247	0.049	13.46	1.34	0.36	Bin*	...
V30	17:38:59.59	-34:34:20.5	14.68	0.16144	0.348	15.27	...	0.26	Bin	...
V31	17:39:01.16	-34:33:12.2	15.77	0.23383	0.322	15.26	0.78	0.22	RR*	...
V32	17:39:01.84	-34:49:41.6	15.68	0.23723	0.474	15.73	0.84	0.24	MISC	...
V33	17:39:03.03	-34:34:15.3	14.68	0.52639	0.093	13.14	0.81	0.24	Bin	...
V34	17:39:06.21	-34:41:41.7	7.21	25.96282	0.118	13.95	1.61	0.47	MISC	...
V35	17:39:10.17	-34:31:43.1	17.20	7.36927	0.092	13.67	1.38	0.40	Bin	...
V36	17:39:12.84	-34:44:37.6	4.50	8.91203	0.096	14.86	1.50	0.41	Bin	...
V37	17:39:13.47	-34:40:25.7	8.61	0.19258	0.430	13.13	0.89	0.26	Bin	...
V38	17:39:14.85	-34:41:43.9	7.42	1.19758	0.272	12.19	0.33	0.03	Bin	P=0.59881
V39	17:39:15.71	-34:31:38.1	17.40	0.12466	0.553	13.62	0.91	0.27	Bin*	...
V40	17:39:21.22	-34:40:02.3	9.53	1.11931	0.086	14.10	1.23	0.39	Bin	MISC; P=0.55964
V41	17:39:21.62	-34:44:08.5	5.97	0.84096	0.189	13.63	0.70	0.24	Bin	...
V42	17:39:22.93	-34:43:02.0	7.06	0.20557	0.172	14.95	0.92	0.25	RR*	...
V43	17:39:24.41	-34:36:38.5	12.99	0.41902	0.270	14.87	1.02	0.31	Bin	...
V44	17:39:29.49	-34:47:04.7	5.86	0.59093	0.192	14.62	0.93	0.29	RR	Bin
V45	17:39:31.18	-34:40:08.5	10.61	0.45602	0.362	14.88	1.04	0.32	RR*	...
V46	17:39:31.58	-34:43:44.3	7.99	0.82798	0.227	13.03	0.59	0.13	Bin	P=0.41489 d
V47	17:39:33.43	-34:48:00.6	6.62	0.46938	0.334	15.08	0.97	0.34	RR	...
V48	17:39:34.52	-34:37:47.0	13.05	0.28486	0.235	14.66	1.64	0.54	Bin	...
V49	17:39:39.15	-34:39:26.3	12.38	31.21711	0.098	14.09	1.50	0.42	MISC	...
V50	17:39:39.48	-34:35:06.6	15.98	0.21359	0.301	14.97	0.86	0.27	Bin	...
V51	17:39:43.53	-34:43:29.1	10.57	0.54353	0.551	15.16	0.83	0.26	Bin	RR
V52	17:39:47.16	-34:40:15.5	13.21	11.67808	0.144	12.98	1.37	0.37	MISC	Bin; P=23.34019
V53	17:39:47.51	-34:43:31.5	11.42	0.21146	0.350	16.07	1.24	0.36	Bin	...

Table 4: Continued.

ID	α_{2000} [hms]	δ_{2000} [dms]	Dist ^a [arcmin]	Period [days]	Amp ^b [mag]	iK_s [mag]	$J - K_s$ [mag]	$H - K_s$ [mag]	Class	Comments (other types/periods)
V54	17:39:47.64	-34:48:30.7	10.12	0.66579	0.233	15.34	0.81	0.24	Bin	...
V55	17:39:48.19	-34:46:30.2	10.53	0.14445	0.627	14.77	0.86	0.22	MISC	Bin; P=0.28891
V56	17:39:48.47	-34:38:39.6	14.53	0.18105	0.233	14.52	14.52	0.34	MISC	Bin; P=0.36210
V57	17:39:48.60	-34:39:40.6	13.86	0.14247	0.288	15.20	MISC	...
V58	17:39:49.25	-34:38:31.3	14.77	6.62427	0.116	13.97	1.63	0.47	Cep*	...
V59	17:39:51.82	-34:49:31.2	11.17	0.21663	0.390	14.38	0.80	0.24	MISC	...
V60	17:39:57.00	-34:45:38.3	8.61	5.32970	0.282	13.94	1.27	0.36	Bin	...
V61	17:39:57.11	-34:44:32.7	13.21	30.33833	0.058	13.24	3.29	2.50	MISC	...
V62	17:39:58.25	-34:38:45.5	16.30	0.18358	0.217	14.61	1.10	0.37	MISC	...
V63	17:39:59.22	-34:47:07.6	13.22	0.61524	0.163	14.83	0.97	0.28	Bin	...
V64	17:40:01.28	-34:40:45.6	15.78	0.31585	0.271	14.78	0.82	0.25	Bin	...
V65	17:40:01.57	-34:36:49.8	18.18	6.85206	0.114	13.62	1.32	0.40	Bin	...
V66	17:40:04.50	-34:45:33.9	14.70	76.75488	0.084	14.02	1.26	0.35	Bin	...
V67	17:40:04.78	-34:39:55.4	16.96	0.44270	0.161	13.96	0.76	0.25	Bin	P=0.22135
V68	17:40:04.89	-34:45:57.9	14.72	0.18533	0.078	13.13	0.91	0.25	Bin	...
V69	17:40:05.48	-34:45:31.4	14.96	0.27276	0.377	14.51	0.61	0.16	MISC	...
V70	17:40:07.25	-34:41:46.2	16.62	0.37462	0.106	13.63	0.72	0.24	Bin	...
V71	17:40:07.59	-34:40:28.1	17.21	0.15041	0.433	15.38	0.93	0.31	δ Sct	...
V72	17:40:09.37	-34:43:47.9	16.36	2.91559	0.109	13.30	1.14	0.33	MISC	Bin; P=5.83089
V73	17:40:13.58	-34:43:44.7	17.38	5.83096	0.183	14.84	1.44	0.46	Bin	P=22.45679
V74	17:38:22.24	-34:21:45.7	11.01	...	0.170	14.62	1.11	0.28	MISC	...
V75	17:38:22.95	-34:46:38.9	11.29	...	0.066	13.51	1.19	0.31	MISC	...
V76	17:38:45.39	-34:27:47.4	18.22	...	0.594	15.47	1.96	0.58	MISC	...
V77	17:38:55.04	-34:30:07.7	14.04	...	0.315	15.01	1.39	0.36	MISC	...
V78	17:38:57.45	-34:29:18.0	14.72	...	0.238	15.16	...	0.56	MISC	...
V79	17:39:22.98	-34:29:16.7	16.41	...	0.250	14.19	1.29	...	MISC	...
V80	17:39:26.48	-34:40:26.5	7.84	...	0.464	15.03	1.58	0.41	MISC	...
V81	17:39:28.21	-34 43:05.3	14.71	...	0.080	13.52	1.33	0.40	MISC	...

^a Distance to the cluster center. ^b K_s total amplitude.

Table 5: List of variable stars found in ESO 393-15

ID	α_{2000} [hms]	δ_{2000} [dms]	Dist ^a [arcmin]	Period [days]	Amp ^b [mag]	iK_s [mag]	$J - K_s$ [mag]	$H - K_s$ [mag]	Class	Comments (other types/periods)
V1	17:43:14.58	-34:13:19.2	5.19	0.58904	0.228	14.47	0.79	0.26	RR*	...
V2	17:43:19.36	-34:10:48.6	4.88	0.18203	0.221	14.89	0.70	0.20	Bin	...
V3	17:43:21.49	-34:14:23.1	3.53	0.16302	0.395	15.13	0.82	0.24	δ Set	...
V4	17:43:22.09	-34:12:10.9	3.61	9.26665	0.108	13.67	0.95	0.26	Bin*	...
V5	17:43:22.45	-34:11:42.9	3.74	12.98331	0.075	13.63	1.20	0.34	MISC	...
V6	17:43:24.76	-34:13:08.6	2.68	3.47711	0.058	14.64	1.08	0.29	MISC	...
V7	17:43:25.80	-34:16:42.2	3.88	0.61680	0.199	14.55	0.77	0.24	Bin/RR	...
V8	17:43:25.81	-34:13:31.4	2.38	0.39748	0.267	14.97	0.73	0.22	Bin	...
V9	17:43:31.30	-34:10:07.5	3.65	35.12639	0.072	14.50	1.19	0.30	Ellipsoidal*	...
V10	17:43:33.39	-34:13:43.8	0.49	0.52252	0.333	12.91	0.60	0.22	MISC	Bin; P=1.04504
V11	17:43:36.01	-34:15:55.0	2.29	0.16241	0.466	15.73	1.66	0.31	Bin	...
V12	17:43:36.62	-34:14:35.0	1.01	0.13454	0.367	14.95	0.89	0.25	RR	Bin; P=0.26908
V13	17:43:36.74	-34:17:06.4	3.49	9.95217	0.133	13.52	1.08	0.31	Bin	P=4.97596
V14	17:43:39.01	-34:12:08.9	1.75	14.83956	0.084	13.65	0.99	0.31	MISC	...
V15	17:43:40.77	-34:16:20.5	3.03	0.59805	0.254	15.24	0.68	0.19	Bin	...
V16	17:43:44.46	-34:11:08.7	3.38	19.94113	0.103	14.60	1.07	0.32	MISC	...
V17	17:43:29.27	-34:15:50.0	2.67	...	0.261	13.89	1.19	0.39	MISC	...
V18	17:43:33.04	-34:09:41.2	3.99	...	0.227	14.59	1.22	0.49	MISC	...

^a Distance to the cluster center. ^b K_s total amplitude.

4. Discussion

Antalova 1 and ASCC 90 are moderately young OCs, while ESO 393-15 is an intermediate-age OC (Table 1). Therefore, it is quite clear that the RR Lyrae stars found in their respective fields must be background stars projected in the direction of the clusters. However, since our project aims at searching variable stars as a whole and in the Galactic OC fields in particular, the classification of such new variables as RR Lyrae stars enlarges not only the sample of RR Lyrae variables currently known but also the background stellar properties to be studied from them.

4.1. Cepheids analysis

We have detected a total of 5 Cepheid candidates in the fields of Antalova 1 and ASCC 90. In order to determine their probability of being cluster members, we calculated their distances and interstellar extinctions by using the period-luminosity (PL) relations in the H and K_s passbands. To determine the type of each Cepheid, we used the PL relations for classical and type II Cepheids. Assuming at first they are classical Cepheids, we used the following PL relations of

Dékány et al. (2015a) adapted to the VVV Survey passbands:

$$M_H = -3.228 [\pm 0.06] \times (\log P - 1) - 5.617 [\pm 0.048], \quad (1)$$

$$M_{K_s} = -3.269 [\pm 0.05] \times (\log P - 1) - 5.663 [\pm 0.048], \quad (2)$$

where M_H and M_{K_s} are the absolute magnitudes in the H and K_s bands, respectively. The color excesses are calculated from:

$$E(H - K_s) = \langle H - K_s \rangle - (M_H - M_{K_s}), \quad (3)$$

where $\langle H - K_s \rangle$ is the mean $(H - K_s)$ color index as defined in Dékány et al. (2015a). The total absorption in the K_s -band and the individual distances R for both Cepheid types were derived from the following relations given by Dékány et al. (2015a):

$$A(K_s) = 1.634 \times E(H - K_s), \quad (4)$$

$$\log R = 1 + 0.2 \times (\langle K_s \rangle - A(K_s) - M_{K_s}), \quad (5)$$

where the mean $\langle K_s \rangle$ magnitudes of the stars were computed from the optimized Fourier fits of the light curves. Secondly, assuming the stars are type II Cepheids, the following PL relations from Matsunaga et al. (2009) were employed:

$$M_H = -2.340 [\pm 0.05] \times (\log P - 1.2) + 14.760 [\pm 0.017], \quad (6)$$

$$M_{K_s} = -2.410 [\pm 0.05] \times (\log P - 1.2) + 14.617 [\pm 0.015]. \quad (7)$$

The results obtained after an analysis of the possible types of Cepheids are shown in Table 6. Since types I and II Cepheids have similar periods and NIR light curves, it is difficult to distinguish their right types in a first approach. Taking into account the K_s reddening map of the VVV bulge obtained by Gonzalez et al. (2011) and Gonzalez et al. (2012), a detailed analysis was recently carried out by Dékány et al. (2015b) examining the coherence in the results obtained for the extinction and distances. We analyzed our results in a similar way and conclude that the possible Cepheids are most likely to be type II from the background fields. These are old population stars lying behind the Galactic bulge.

Table 6: Observed and derived parameters for the 5 Cepheid candidates of the two possible types

ID	$\langle K_s \rangle$	$\langle H - K_s \rangle$	$E(H - K_s)_I$	$(A_{K_s})_I$	Dist _I [pc]	$E(H - K_s)_{II}$	$(A_{K_s})_{II}$	Dist _{II} [pc]
V11-Cls1	13.770	0.475	0.433	0.708	47133	0.384	0.627	18307
V21-Cls1	12.991	0.369	0.330	0.540	31924	0.283	0.462	12738
V38-Cls1	13.113	0.611	0.565	0.924	36835	0.512	0.837	13767
V11-Cls2	13.682	0.608	0.568	0.928	38447	0.520	0.849	15164
V58-Cls2	13.973	0.467	0.428	0.700	46803	0.381	0.621	18657

4.2. *Eclipsing binaries analysis*

From the whole sample of binary system candidates, we selected the most probable ones and determined the physical parameters of the eclipsing components. We first used the Wilson & Devinney (WD) code (Wilson and Van Hamme, 2014), which operates in two steps while fitting the light curves, i.e., the LC (a subjective iteration) and the DC (an objective iteration) processes. The LC procedure is based on parameters previously determined from theory or observation (Wilson, 1994b,a, 2001, 2006). On the other hand, the DC is the differential calculus which aims at better determining the geometrical and physical parameters of the systems by reducing possible associated errors. Light curves were first analyzed by the LC procedure using known parameters, such as the period. The output file was then used as input for the DC procedure. The effectiveness of the WD code is not particularly favorable since it is time consuming so, as we intend to study many objects, we searched for another method. Currently, there are several graphical user interface programs that can be used for a scientific study of these objects. Among them, we tested the PHOEBE (PHysics Of Eclipsing BinariEs) program. This is a tool for modeling eclipsing binary stars based on photometric and spectroscopic (radial velocity) data, which is also based on the WD code. PHOEBE can determine the parameters associated with the physical and geometrical conditions of the system, like in the WD code. It can also deal with the parameters of the binary components to which we have access once the values associated with the obtained light-curves were determined.

We used both WD and PHOEBE codes for our analysis and probed different classification modes. Taking into account the shape of the light curves, we conclude that the systems involved are detached, semi-detached or close contact binary systems. The best fittings of the corresponding light curves are shown in Figures 8 - 10. Table 7 shows the resulting parameters that could be obtained from the current analysis. M_2/M_1 represents the mass ratio between the components.

We would like to point out that, in general terms, the studied systems exhibit orbits that are almost circular, their eccentricities being about 5×10^{-4} . The stars involved seem to have solar or higher than solar surface temperatures.

Table 7: Model and fixed parameters for the selected eclipsing binary stars.

Eclipsing Binary	Object Type	Period [days]	Inclination [°] (± 1.1)	Eccentricity (± 0.006)	T_1 [K]	T_2 [K]	M_2/M_1 (± 0.07)
V17-Cls1	Detached	1.7956	72.9	0.004	2900 \pm 80	2420 \pm 70	0.97
V19-Cls1	Detached	38.0	75	0.000	8400 \pm 400	5000 \pm 200	0.69
V35-Cls1	Double-contact	0.5163	77	0.009	3200 \pm 200	2900 \pm 200	0.80
V15-Cls2	Semi-detached	0.5679	89	0.010	8000 \pm 400	5000 \pm 500	1.77
V18-Cls2	Double-contact	0.3108	90	0.001	5000 \pm 200	4500 \pm 400	0.80
V25-Cls2	Double-contact	0.7699	73.5	0.005	6000 \pm 70	5800 \pm 100	1.41
V40-Cls2	Semi-detached	1.1193	63.5	0.005	7000 \pm 1000	3500 \pm 900	1.40
V51-Cls2	Semi-detached	0.5435	90	0.000	6000 \pm 200	8000 \pm 200	1.80
V60-Cls2	Semi-detached	5.3298	68	0.000	7000 \pm 1000	5600 \pm 600	0.79
V13-Cls3	Double-contact	9.9522	50	0.000	3340 \pm 60	2950 \pm 50	0.80
V15-Cls3	Double-contact	0.5980	68	0.000	4800 \pm 80	3500 \pm 30	0.90

Since the cross-match is purely positional, most of the newly discovered variable stars are not cluster members but part of the bulge population projected onto the clusters' fields, such as RR Lyrae stars and the Cepheids found. According to the CMDs, we can obtain possible candidates for the clusters' members. In ASCC 90 we found 43 possible EBs. However, only 8 of these binaries might be cluster members. In Antalova 1, from 18 new found EBs, only 6 candidates could be cluster members and in ESO 393-15, from 18 BEs found in its region, only 3 of them might be cluster member candidates. The rest of the EBs found in ESO 393-15 are probably background objects because they appear to have much redder colors than the corresponding cluster isochrone. Besides the detected variability and deep photometry, the good spatial resolution of the VVV Survey also allows for proper motion studies to be carried out in the future when a longer baseline becomes available. A further spectroscopic study is planned to obtain radial velocities which will help us to confirm or deny the physical association of the variables found to the corresponding clusters. The search in both cases, extended and compact OCs, present benefits as well as disadvantages. While the probabilities of finding variable stars in extended clusters are higher, their decontamination processes are more complicated, and the probabilities of containing

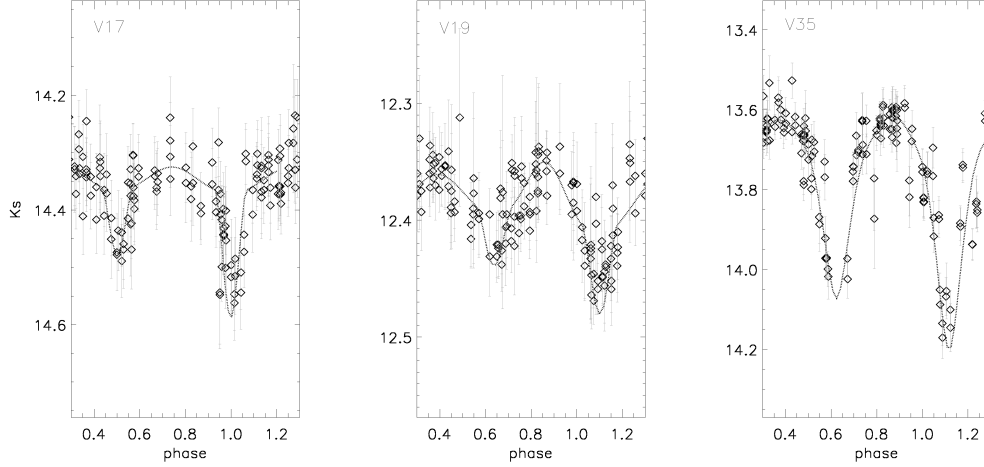


Figure 8: Light curves of the best binaries found in the field of Antalova 1. Solid lines represent the best fittings of the observed light curves for the eclipsing binary stars. Diamonds stand for the observed $\langle K_s \rangle$ magnitudes taken from the VVV Survey.

field stars existing in the cluster regions are also higher. Our project intends to find the possible variables belonging to the host clusters, as well as to complete the search in the NIR bands and characterize the field variable stars. In our view, determining cluster membership is a difficult issue, contamination by background variable stars is a major problem and we believe that most of the variables found in the fields of the OCs studied here appear not to be associated with such OCs. A definite way to secure membership would be the use of kinematic data. Unfortunately, the radial velocities of these three clusters are largely unknown and quite telescope time consuming to obtain. However, their proper motions may be measured instead using the same VVV data. The accuracy of the proper motions measured by VVV astrometry has been estimated to be ~ 2 mas/yr Libralato et al. 2015. Such precision is not enough to secure cluster membership. We need to increase the time baseline for some more years in order to obtain good and reliable (at least statistically) proper motions for the OCs of our study.

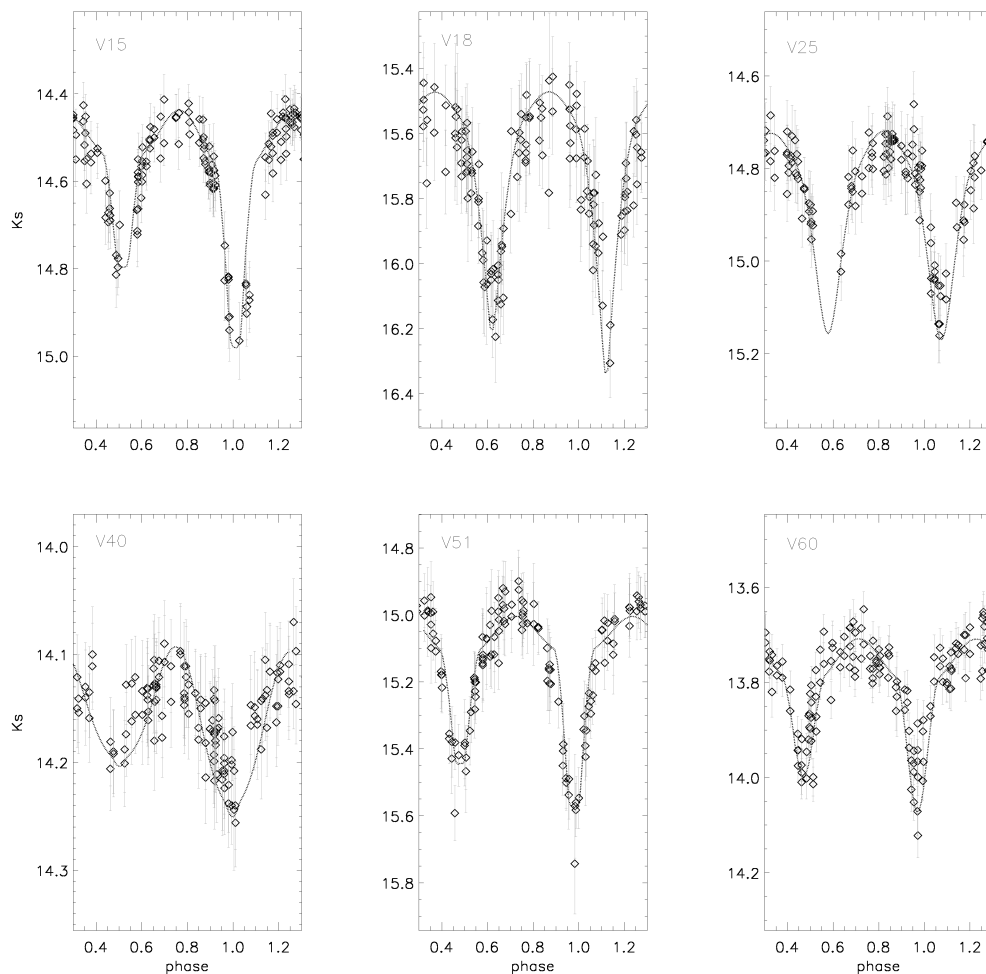


Figure 9: Light curves of the best binaries found in the field of ASCC 90. Lines and symbols represent the same as in Figure 8.

5. Conclusions

We have presented a new search for variable stars in the fields of three studied OCs using the NIR database of the VVV Survey. We have defined the procedures for variable stars search in VVV OCs. In this final section, a brief summary of our findings is presented.

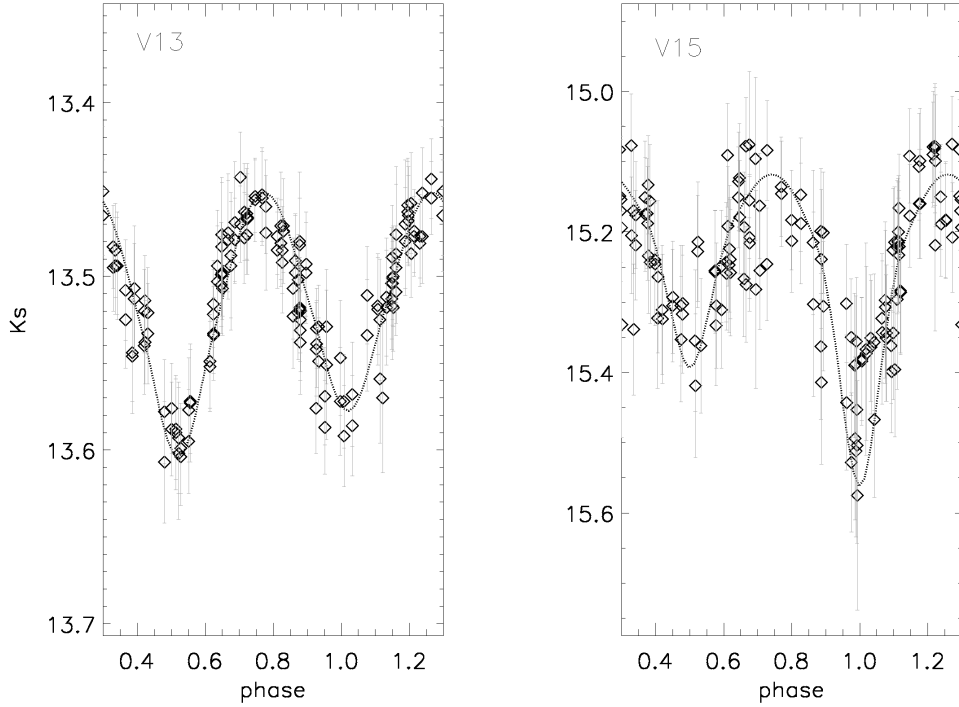


Figure 10: Light curves of the best binaries found in the field of ESO 393-15. Lines and symbols represent the same as in Figure 8.

- We found 5 new Cepheids in the cluster fields, none of which appear to be cluster members. A large number of background RR Lyrae stars in the fields of the three studied clusters have also been found.
- We identified a large number of EBs in the cluster fields. A total of 17, 42, and 8 EBs were found in the fields of Antalova 1, ASCC 90 and ESO 393-15, respectively. Based on NIR CMDs, we recognized only 8, 6, and 6 of such EBs as probable members of Antalova 1, ASCC 90 and ESO 393-15, respectively. We obtained fundamental parameters for some selected EBs. They were classified as detached, semi-detached and/or double-contact binaries, with low eccentricities and high inclinations. Future spectroscopic follow-up of some of these binary systems may help to confirm cluster

membership and also to obtain heliocentric distances to the clusters.

- Our experience shows that for clusters projected onto highly reddened and obscured regions of the bulge, it is very hard to decontaminate the CMDs. Another major problem is to discriminate cluster members from field stars.
- Lastly, it has not been possible to determine the variable type of some objects. That is mainly due to their lack of periodicity and to our inability to phase them using the current data. Therefore, they remain unclassified.

Acknowledgements

We gratefully acknowledge the use of data from the ESO Public Survey program 179.B-2002 taken with the VISTA 4.1 m telescope and data products from the Cambridge Astronomical Survey Unit. Support for TP, DM, ID and JAG is provided by the Ministry of Economy, Development, and Tourism's Millennium Science Initiative through grant IC120009, awarded to the Millennium Institute of Astrophysics, MAS. TP, JJC and LVG acknowledge financial support from the Argentinian institutions FONCYT, CONICET and SECYT (Universidad Nacional de Córdoba). DM is also supported by the Center for Astrophysics and Associated Technologies PFB-06, and Fondecyt Project No. 1130196. JAG acknowledges support from the FIC-R Fund, allocated to the project 30321072, by CONICYT's PCI program through grant DPI20140066 and from Fondecyt Iniciación 11150916. This research has made use of the SIMBAD database, operated at CDS, Strasbourg, France; also the SAO/NASA Astrophysics data (ADS).

6. References

- Alonso-García, J., Dékány, I., Catelan, M., Contreras Ramos, R., Gran, F., Amigo, P., Leyton, P., Minniti, D., Mar. 2015. Variable Stars in the VVV Globular Clusters. I. 2MASS-GC 02 and Terzan 10. *AJ*149, 99.
- Alonso-García, J., Mateo, M., Sen, B., Banerjee, M., Catelan, M., Minniti, D., von Braun, K., Mar. 2012. Uncloaking Globular Clusters in the Inner Galaxy. *AJ*143, 70.
- Archinal, B. A., Hynes, S. J., 2003. *Star clusters*. Willman Bell, Inc.

- Barbá, R. H., Roman-Lopes, A., Nilo Castellón, J. L., Firpo, V., Minniti, D., Lucas, P., Emerson, J. P., Hempel, M., Soto, M., Saito, R. K., Sep. 2015. Hundreds of new cluster candidates in the VISTA Variables in the Vía Láctea survey DR1. *A&A*581, A120.
- Bica, E., Bonatto, C., Blumberg, R., Dec. 2006. Faint open clusters with 2MASS: BH 63, Lyngå 2, Lyngå 12 and King 20. *A&A*460, 83–92.
- Bica, E., Dutra, C. M., Soares, J., Barbuy, B., Jun. 2003. New infrared star clusters in the Northern and Equatorial Milky Way with 2MASS. *A&A*404, 223–232.
- Borissova, J., Bonatto, C., Kurtev, R., Clarke, J. R. A., Peñaloza, F., Sale, S. E., Minniti, D., Alonso-García, J., Artigau, E., Barbá, R., Bica, E., Baume, G. L., Catelan, M., Chenè, A. N., Dias, B., Folkes, S. L., Froebrich, D., Geisler, D., de Grijs, R., Hanson, M. M., Hempel, M., Ivanov, V. D., Kumar, M. S. N., Lucas, P., Mauro, F., Moni Bidin, C., Rejkuba, M., Saito, R. K., Tamura, M., Toledo, I., Aug. 2011. New Galactic star clusters discovered in the VVV survey. *A&A*532, A131.
- Borissova, J., Chené, A.-N., Ramírez Alegría, S., Sharma, S., Clarke, J. R. A., Kurtev, R., Negueruela, I., Marco, A., Amigo, P., Minniti, D., Bica, E., Bonatto, C., Catelan, M., Fierro, C., Geisler, D., Gromadzki, M., Hempel, M., Hanson, M. M., Ivanov, V. D., Lucas, P., Majaess, D., Moni Bidin, C., Popescu, B., Saito, R. K., Sep. 2014. New galactic star clusters discovered in the VVV survey. Candidates projected on the inner disk and bulge. *A&A*569, A24.
- Bressan, A., Marigo, P., Girardi, L., Salasnich, B., Dal Cero, C., Rubele, S., Nanni, A., Nov. 2012. PARSEC: stellar tracks and isochrones with the PAdova and TRieste Stellar Evolution Code. *MNRAS*427, 127–145.
- Chen, L., Hou, J. L., Wang, J. J., Mar. 2003. On the Galactic Disk Metallicity Distribution from Open Clusters. I. New Catalogs and Abundance Gradient. *AJ*125, 1397–1406.
- Chené, A.-N., Borissova, J., Bonatto, C., Majaess, D. J., Baume, G., Clarke, J. R. A., Kurtev, R., Schnurr, O., Bouret, J.-C., Catelan, M., Emerson, J. P., Feinstein, C., Geisler, D., de Grijs, R., Hervé, A., Ivanov, V. D., Kumar, M. S. N., Lucas, P., Mahy, L., Martins, F., Mauro, F., Minniti, D., Moni Bidin, C., Jan. 2013. Massive open star clusters using the VVV survey. II. Discovery of six clusters with Wolf-Rayet stars. *A&A*549, A98.

- Conrad, C., Scholz, R.-D., Kharchenko, N. V., Piskunov, A. E., Schilbach, E., Röser, S., Boeche, C., Kordopatis, G., Siebert, A., Williams, M., Munari, U., Matijevič, G., Grebel, E. K., Zwitter, T., de Jong, R. S., Steinmetz, M., Gilmore, G., Seabroke, G., Freeman, K., Navarro, J. F., Parker, Q., Reid, W., Watson, F., Gibson, B. K., Bienaymé, O., Wyse, R., Bland-Hawthorn, J., Siviero, A., Feb. 2014. A RAVE investigation on Galactic open clusters. I. Radial velocities and metallicities. *A&A*562, A54.
- Dalton, G. B., Caldwell, M., Ward, A. K., Whalley, M. S., Woodhouse, G., Edeson, R. L., Clark, P., Beard, S. M., Gallie, A. M., Todd, S. P., Strachan, J. M. D., Bezawada, N. N., Sutherland, W. J., Emerson, J. P., Jun. 2006. The VISTA infrared camera. In: Society of Photo-Optical Instrumentation Engineers (SPIE) Conference Series. Vol. 6269 of Society of Photo-Optical Instrumentation Engineers (SPIE) Conference Series. p. 0.
- Dékány, I., Minniti, D., Catelan, M., Zoccali, M., Saito, R. K., Hempel, M., Gonzalez, O. A., Oct. 2013. VVV Survey Near-infrared Photometry of Known Bulge RR Lyrae Stars: The Distance to the Galactic Center and Absence of a Barred Distribution of the Metal-poor Population. *ApJ*776, L19.
- Dékány, I., Minniti, D., Hajdu, G., Alonso-García, J., Hempel, M., Palma, T., Catelan, M., Gieren, W., Majaess, D., Jan. 2015a. Discovery of a Pair of Classical Cepheids in an Invisible Cluster Beyond the Galactic Bulge. *ApJ*799, L11.
- Dékány, I., Minniti, D., Majaess, D., Zoccali, M., Hajdu, G., Alonso-García, J., Catelan, M., Gieren, W., Borissova, J., Oct. 2015b. The VVV Survey Reveals Classical Cepheids Tracing a Young and Thin Stellar Disk across the Galaxy Bulge. *ApJ*812, L29.
- Dutra, C. M., Bica, E., Soares, J., Barbuy, B., Mar. 2003. New infrared star clusters in the southern Milky Way with 2MASS. *A&A*400, 533–539.
- Emerson, J. P., Irwin, M. J., Lewis, J., Hodgkin, S., Evans, D., Bunclark, P., McMahon, R., Hambly, N. C., Mann, R. G., Bond, I., Sutorius, E., Read, M., Williams, P., Lawrence, A., Stewart, M., Sep. 2004. VISTA data flow system: overview. In: Quinn, P. J., Bridger, A. (Eds.), *Optimizing Scientific Return for Astronomy through Information Technologies*. Vol. 5493 of Society of Photo-Optical Instrumentation Engineers (SPIE) Conference Series. pp. 401–410.
- Friel, E. D., 1995. The Old Open Clusters Of The Milky Way. *ARA&A*33, 381–414.

- Gonzalez, O. A., Rejkuba, M., Zoccali, M., Valenti, E., Minniti, D., Oct. 2011. Reddening and metallicity maps of the Milky Way bulge from VVV and 2MASS. I. The method and minor axis maps. *A&A*534, A3.
- Gonzalez, O. A., Rejkuba, M., Zoccali, M., Valenti, E., Minniti, D., Schultheis, M., Tobar, R., Chen, B., Jul. 2012. Reddening and metallicity maps of the Milky Way bulge from VVV and 2MASS. II. The complete high resolution extinction map and implications for Galactic bulge studies. *A&A*543, A13.
- Hambly, N. C., Mann, R. G., Bond, I., Sutorius, E., Read, M., Williams, P., Lawrence, A., Emerson, J. P., Sep. 2004. VISTA data flow system survey access and curation: the WFCAM science archive. In: Quinn, P. J., Bridger, A. (Eds.), *Optimizing Scientific Return for Astronomy through Information Technologies*. Vol. 5493 of Society of Photo-Optical Instrumentation Engineers (SPIE) Conference Series. pp. 423–431.
- Irwin, M. J., Lewis, J., Hodgkin, S., Bunclark, P., Evans, D., McMahon, R., Emerson, J. P., Stewart, M., Beard, S., Sep. 2004. VISTA data flow system: pipeline processing for WFCAM and VISTA. In: Quinn, P. J., Bridger, A. (Eds.), *Optimizing Scientific Return for Astronomy through Information Technologies*. Vol. 5493 of Society of Photo-Optical Instrumentation Engineers (SPIE) Conference Series. pp. 411–422.
- Kharchenko, N. V., Piskunov, A. E., Röser, S., Schilbach, E., Scholz, R.-D., Sep. 2005a. 109 new Galactic open clusters. *A&A*440, 403–408.
- Kharchenko, N. V., Piskunov, A. E., Röser, S., Schilbach, E., Scholz, R.-D., Aug. 2005b. Astrophysical parameters of Galactic open clusters. *A&A*438, 1163–1173, (K05).
- Kharchenko, N. V., Piskunov, A. E., Schilbach, E., Röser, S., Scholz, R.-D., Oct. 2013. Global survey of star clusters in the Milky Way. II. The catalogue of basic parameters. *A&A*558, A53, (K13).
- Libralato, M., Bellini, A., Bedin, L. R., Anderson, J., Piotto, G., Nascimbeni, V., Platais, I., Minniti, D., Zoccali, M., Jun. 2015. High-precision astrometry with VVV - I. An independent reduction pipeline for VIRCAM@VISTA. *MNRAS*450, 1664–1673.
- Matsunaga, N., Feast, M. W., Menzies, J. W., Aug. 2009. Period-luminosity relations for type II Cepheids and their application. *MNRAS*397, 933–942.

- Minniti, D., Lucas, P. W., Emerson, J. P., Saito, R. K., Hempel, M., Pietrukowicz, P., Ahumada, A. V., Alonso, M. V., Alonso-Garcia, J., Arias, J. I., Bandyopadhyay, R. M., Barbá, R. H., Barbuy, B., Bedin, L. R., Bica, E., Borissova, J., Bronfman, L., Carraro, G., Catelan, M., Clariá, J. J., Cross, N., de Grijs, R., Dékány, I., Drew, J. E., Fariña, C., Feinstein, C., Fernández Lajús, E., Gamen, R. C., Geisler, D., Gieren, W., Goldman, B., Gonzalez, O. A., Gunthardt, G., Gurovich, S., Hambly, N. C., Irwin, M. J., Ivanov, V. D., Jordán, A., Kerins, E., Kinemuchi, K., Kurtev, R., López-Corredoira, M., Maccarone, T., Masetti, N., Merlo, D., Messineo, M., Mirabel, I. F., Monaco, L., Morelli, L., Padilla, N., Palma, T., Parisi, M. C., Pignata, G., Rejkuba, M., Roman-Lopes, A., Sale, S. E., Schreiber, M. R., Schröder, A. C., Smith, M., , Jr., L. S., Soto, M., Tamura, M., Tappert, C., Thompson, M. A., Toledo, I., Zoccali, M., Pietrzynski, G., Jul. 2010. VISTA Variables in the Via Lactea (VVV): The public ESO near-IR variability survey of the Milky Way. *New A*15, 433–443.
- Portegies Zwart, S. F., McMillan, S. L. W., Gieles, M., Sep. 2010. Young Massive Star Clusters. *ARA&A*48, 431–493.
- Ramírez Alegría, S., Borissova, J., Chené, A.-N., Bonatto, C., Kurtev, R., Amigo, P., Kuhn, M., Gromadzki, M., Carballo-Bello, J. A., Apr. 2016. Massive open star clusters using the VVV survey. V. Young clusters with an OB stellar population. *A&A*588, A40.
- Ramírez Alegría, S., Borissova, J., Chené, A. N., O’Leary, E., Amigo, P., Minniti, D., Saito, R. K., Geisler, D., Kurtev, R., Hempel, M., Gromadzki, M., Clarke, J. R. A., Negueruela, I., Marco, A., Fierro, C., Bonatto, C., Catelan, M., Apr. 2014. Massive open star clusters using the VVV survey. III. A young massive cluster at the far edge of the Galactic bar. *A&A*564, L9.
- Roeser, S., Demleitner, M., Schilbach, E., Jun. 2010. The PPMXL Catalog of Positions and Proper Motions on the ICRS. Combining USNO-B1.0 and the Two Micron All Sky Survey (2MASS). *AJ*139, 2440–2447.
- Saito, R. K., Hempel, M., Minniti, D., Lucas, P. W., Rejkuba, M., Toledo, I., Gonzalez, O. A., Alonso-García, J., Irwin, M. J., Gonzalez-Solares, E., Hodgkin, S. T., Lewis, J. R., Cross, N., Ivanov, V. D., Kerins, E., Emerson, J. P., Soto, M., Amôres, E. B., Gurovich, S., Dékány, I., Angeloni, R., Beamin, J. C., Catelan, M., Padilla, N., Zoccali, M., Pietrukowicz, P., Moni Bidin, C., Mauro, F., Geisler, D., Folkes, S. L., Sale, S. E., Borissova, J., Kurtev, R., Ahumada,

A. V., Alonso, M. V., Adamson, A., Arias, J. I., Bandyopadhyay, R. M., Barbá, R. H., Barbuy, B., Baume, G. L., Bedin, L. R., Bellini, A., Benjamin, R., Bica, E., Bonatto, C., Bronfman, L., Carraro, G., Chenè, A. N., Clariá, J. J., Clarke, J. R. A., Contreras, C., Corvillón, A., de Grijs, R., Dias, B., Drew, J. E., Fariña, C., Feinstein, C., Fernández-Lajús, E., Gamen, R. C., Gieren, W., Goldman, B., González-Fernández, C., Grand, R. J. J., Gunthardt, G., Hambly, N. C., Hanson, M. M., Hełminiak, K. G., Hoare, M. G., Huckvale, L., Jordán, A., Kinemuchi, K., Longmore, A., López-Corredoira, M., Maccarone, T., Majaess, D., Martín, E. L., Masetti, N., Mennickent, R. E., Mirabel, I. F., Monaco, L., Morelli, L., Motta, V., Palma, T., Parisi, M. C., Parker, Q., Peñaloza, F., Pietrzyński, G., Pignata, G., Popescu, B., Read, M. A., Rojas, A., Roman-Lopes, A., Ruiz, M. T., Saviane, I., Schreiber, M. R., Schröder, A. C., Sharma, S., Smith, M. D., Sodrè, L., Stead, J., Stephens, A. W., Tamura, M., Tappert, C., Thompson, M. A., Valenti, E., Vanzì, L., Walton, N. A., Weidmann, W., Zijlstra, A., Jan. 2012. VVV DR1: The first data release of the Milky Way bulge and southern plane from the near-infrared ESO public survey VISTA variables in the Vía Láctea. *A&A*537, A107.

Skrutskie, M. F., Cutri, R. M., Stiening, R., Weinberg, M. D., Schneider, S., Carpenter, J. M., Beichman, C., Capps, R., Chester, T., Elias, J., Huchra, J., Liebert, J., Lonsdale, C., Monet, D. G., Price, S., Seitzer, P., Jarrett, T., Kirkpatrick, J. D., Gizis, J. E., Howard, E., Evans, T., Fowler, J., Fullmer, L., Hurt, R., Light, R., Kopan, E. L., Marsh, K. A., McCallon, H. L., Tam, R., Van Dyk, S., Wheelock, S., Feb. 2006. The Two Micron All Sky Survey (2MASS). *AJ*131, 1163–1183.

Steinmetz, M., Zwitter, T., Siebert, A., Watson, F. G., Freeman, K. C., Munari, U., Campbell, R., Williams, M., Seabroke, G. M., Wyse, R. F. G., Parker, Q. A., Bienaymé, O., Roeser, S., Gibson, B. K., Gilmore, G., Grebel, E. K., Helmi, A., Navarro, J. F., Burton, D., Cass, C. J. P., Dawe, J. A., Fiegert, K., Hartley, M., Russell, K. S., Saunders, W., Enke, H., Bailin, J., Binney, J., Bland-Hawthorn, J., Boeche, C., Dehnen, W., Eisenstein, D. J., Evans, N. W., Fiorucci, M., Fulbright, J. P., Gerhard, O., Jauregi, U., Kelz, A., Mijović, L., Minchev, I., Parmentier, G., Peñarrubia, J., Quillen, A. C., Read, M. A., Ruchti, G., Scholz, R.-D., Siviero, A., Smith, M. C., Sordo, R., Veltz, L., Vidrih, S., von Berlepsch, R., Boyle, B. J., Schilbach, E., Oct. 2006. The Radial Velocity Experiment (RAVE): First Data Release. *AJ*132, 1645–1668.

- Stellingwerf, R. F., Sep. 1978. Period determination using phase dispersion minimization. *ApJ*224, 953–960.
- Stetson, P. B., Oct. 1996. On the Automatic Determination of Light-Curve Parameters for Cepheid Variables. *PASP*108, 851.
- Trumpler, R. J., 1930. Preliminary results on the distances, dimensions and space distribution of open star clusters. *Lick Observatory Bulletin* 14, 154–188.
- Valenti, E., Ferraro, F. R., Origlia, L., Apr. 2007. Near-Infrared Properties of 24 Globular Clusters in the Galactic Bulge. *AJ*133, 1287–1301.
- Wilson, R. E., Sep. 1994a. Binary-star light curve models. *PASP*106, 921–941.
- Wilson, R. E., Mar. 1994b. Invited Review Paper Understanding Binary Stars Via Light Curves. *International Amateur-Professional Photoelectric Photometry Communications* 55, 1.
- Wilson, R. E., May 2001. Binary Star Morphology and the Name Overcontact. *Information Bulletin on Variable Stars* 5076.
- Wilson, R. E., Apr. 2006. Binary Stars and their Light Curves. In: Aerts, C., Sterken, C. (Eds.), *Astrophysics of Variable Stars*. Vol. 349 of *Astronomical Society of the Pacific Conference Series*. p. 71.
- Wilson, R. E., Van Hamme, W., Jan. 2014. Unification of Binary Star Ephemeris Solutions. *ApJ*780, 151.
- Zechmeister, M., Kürster, M., Mar. 2009. The generalised Lomb-Scargle periodogram. A new formalism for the floating-mean and Keplerian periodograms. *A&A*496, 577–584.
- Zejda, M., Paunzen, E., Baumann, B., Mikulášek, Z., Liška, J., Dec. 2012. Catalogue of variable stars in open cluster fields. *A&A*548, A97, (Z12).